$Ca_V1.2/Ca_V3.x$ channels mediate divergent vasomotor responses in human cerebral arteries

Osama F. Harraz,[1,4] Frank Visser,[2] Suzanne E. Brett,[1] Daniel Goldman,[5] Anil Zechariah,[1] Ahmed M. Hashad,[1] Bijoy K. Menon,[3] Tim Watson,[3] Yves Starreveld,[3] and Donald G. Welsh[1]

[1]Department of Physiology and Pharmacology, Hotchkiss Brain and Libin Cardiovascular Institutes, and [2]Molecular Core Facility, Hotchkiss Brain Institute, and [3]Department of Clinical Neurosciences, University of Calgary, Calgary, Alberta T2N 4N1, Canada
[4]Department of Pharmacology and Toxicology, Faculty of Pharmacy, Alexandria University, Alexandria 21521, Egypt
[5]Department of Medical Biophysics, University of Western Ontario, London, Ontario N6A 5C1, Canada

The regulation of arterial tone is critical in the spatial and temporal control of cerebral blood flow. Voltage-gated Ca^{2+} (Ca_V) channels are key regulators of excitation–contraction coupling in arterial smooth muscle, and thereby of arterial tone. Although L- and T-type Ca_V channels have been identified in rodent smooth muscle, little is known about the expression and function of specific Ca_V subtypes in human arteries. Here, we determined which Ca_V subtypes are present in human cerebral arteries and defined their roles in determining arterial tone. Quantitative polymerase chain reaction and Western blot analysis, respectively, identified mRNA and protein for L- and T-type channels in smooth muscle of cerebral arteries harvested from patients undergoing resection surgery. Analogous to rodents, $Ca_V1.2$ (L-type) and $Ca_V3.2$ (T-type) α_1 subunits were expressed in human cerebral arterial smooth muscle; intriguingly, the $Ca_V3.1$ (T-type) subtype present in rodents was replaced with a different T-type isoform, $Ca_V3.3$, in humans. Using established pharmacological and electrophysiological tools, we separated and characterized the unique profiles of Ca^{2+} channel subtypes. Pressurized vessel myography identified a key role for $Ca_V1.2$ and $Ca_V3.3$ channels in mediating cerebral arterial constriction, with the former and latter predominating at higher and lower intraluminal pressures, respectively. In contrast, $Ca_V3.2$ antagonized arterial tone through downstream regulation of the large-conductance Ca^{2+}-activated K^+ channel. Computational analysis indicated that each Ca^{2+} channel subtype will uniquely contribute to the dynamic regulation of cerebral blood flow. In conclusion, this study documents the expression of three distinct Ca^{2+} channel subtypes in human cerebral arteries and further shows how they act together to orchestrate arterial tone.

The Journal of General Physiology

INTRODUCTION

The spatial and temporal distribution of brain blood flow is set by networks of resistance arteries. Cerebral arteries are responsive to a range of humoral and mechanical stimuli (Furchgott and Zawadzki, 1980; Segal, 2000; Filosa et al., 2006), one of the key being arterial pressure (Knot and Nelson, 1998). Under dynamic conditions, elevated intraluminal pressure initiates arterial constriction by modulating ionic conductances that depolarize arterial smooth muscle membrane potential (V_M) (Knot and Nelson, 1998; Welsh et al., 2000, 2002). This electrical event in turn grades the opening of voltage-gated Ca^{2+} (Ca_V) channels, and the subsequent rise in cytosolic $[Ca^{2+}]_i$ triggers the activation of myosin light chain kinase and actin–myosin cross-bridge cycling (Gallagher et al., 1997; Cole and Welsh, 2011). As Ca_V channels play a key role in setting arterial tone, these channels have long been a target of therapeutic interest, with blockers commonly used to moderate systemic hypertension and cerebral vasospasm (Godfraind, 2014).

The Ca_V channel family comprises 10 α_1 pore–forming subtypes, among which the $Ca_V1.2$ channel predominates in the transduction of vascular smooth muscle contractility (Catterall, 2011). Given the robust vasodilatory response to L-type blockers (e.g., dihydropyridines), it is often assumed that this channel is the sole subtype expressed in rodent and human arteries (Knot and Nelson, 1998; Moosmang et al., 2003). Although a principal conductance, emerging animal studies indicate the presence of additional subtypes (Jensen et al., 2004; Kuo et al., 2010; Abd El-Rahman et al., 2013). Of particular note are T-type Ca^{2+} channels whose voltage profiles are leftward shifted, compared with L-type, positioning them to be more active at hyperpolarized V_M. Initial data argued that T-type channels were functionally similar to L-type in elevating cytosolic $[Ca^{2+}]_i$, albeit at

Correspondence to Donald G. Welsh: dwelsh@ucalgary.ca

Abbreviations used in this paper: BK_{Ca}, large-conductance Ca^{2+}-activated K^+; Ca_V, voltage-gated Ca^{2+}; PSS, physiological saline solution; qPCR, quantitative PCR; STOC, spontaneous transient outward K^+ current; V_M, membrane potential.

The Rockefeller University Press $30.00
J. Gen. Physiol. Vol. 145 No. 5 405–418
www.jgp.org/cgi/doi/10.1085/jgp.201511361

lower intraluminal pressures where arteries are hyperpolarized (Abd El-Rahman et al., 2013; Björling et al., 2013). Recent reports, however, indicate that T-type regulation of arterial tone is more sophisticated, with one subtype ($Ca_V3.1$) driving constrictor responses and the other ($Ca_V3.2$) mediating feedback dilation (Chen et al., 2003; Harraz et al., 2014; Thuesen et al., 2014). These animal observations are intriguing, but their translational significance has remained elusive as mechanistic studies have not extended to the human vasculature.

The goal of this study was to delineate Ca^{2+} channels in native human cerebral arterial smooth muscle and to determine how each conductance modulates arterial tone development. We hypothesized that both L- and T-type Ca^{2+} channels are present and that each conductance mediates distinctive vasomotor responses. Our investigation progressed from cells to tissues and involved the integrative use of pressurized myography, Western blot analysis, PCR, electrophysiology, and computational modeling. In human cerebral arterial smooth muscle cells, we documented for the first time the expression of L- ($Ca_V1.2$) and T-type ($Ca_V3.2$/$Ca_V3.3$) channels and characterized their unique physiological and pharmacological profiles. Subsequent observations showed that $Ca_V1.2$ and $Ca_V3.3$ augmented myogenic arterial tone in a manner consistent with their voltage dependence. In stark contrast, human $Ca_V3.2$ antagonized tone development and enabled indirect arterial vasodilation through its influence on large-conductance Ca^{2+}-activated K^+ (BK_{Ca}) channels. The divergent roles of Ca^{2+} channels are therapeutically important, as subtype-specific targeting could either suppress or enhance arterial tone. In summary, this human-based study is the first to illustrate the expression of three different Ca_V channels and to encode their distinctive influences on human cerebral arterial tone development.

MATERIALS AND METHODS

Human tissues and animal procedures

Excised human brain samples were obtained after institutional review board approval, written informed consent, and in accordance with the guidelines of the Declaration of Helsinki. Brain tissues were collected and placed in cold PBS, pH 7.4, containing (mM) 138 NaCl, 3 KCl, 10 Na_2HPO_4, 2 NaH_2PO_4, 5 glucose, 0.1 $CaCl_2$, and 0.1 $MgSO_4$, and transferred to the laboratory. Small superficial cerebral arteries (~150–250-µm diameter) were carefully dissected out of surrounding tissue and cut into segments. Animal procedures were approved by the Animal Care and Use Committee at the University of Calgary. In brief, female Sprague–Dawley rats (2–4-mo old) or C57BL/6 mice (2–4-mo old) were euthanized via CO_2 asphyxiation. The brain was carefully removed and placed in cold PBS. Middle and posterior cerebral arteries were carefully dissected out of surrounding tissue and cut into ~2-mm segments for enzymatic digestion.

Pressurized vessel myography

Human arterial segments were mounted in a customized arteriograph and superfused with warm (37°C) physiological saline solution (PSS) containing: 119 mM NaCl, 4.7 mM KCl, 20 mM $NaHCO_3$, 1.1 mM KH_2PO_4, 1.2 mM $MgSO_4$, 1.6 mM $CaCl_2$, and 10 mM glucose, pH 7.4 (21% O_2, 5% CO_2, balance N_2). To limit the endothelial feedback influence on myogenic tone development, air bubbles were passed through the vessel lumen (1–2 min). Arteries were equilibrated at 15 mmHg, and the contractile responsiveness was assessed by brief application of 60 mM KCl. After equilibration, intraluminal pressure was incrementally elevated from 20 to 100 mmHg and arterial external diameter was monitored under control conditions and in the presence of 200 nM nifedipine ($Ca_V1.2$ inhibitor), 1 µM NNC 55–0396 (T-type blocker), and/or 50 µM Ni^{2+} ($Ca_V3.2$ blocker). Maximal arterial diameter was subsequently assessed in Ca^{2+}-free PSS (zero externally added Ca^{2+} plus 2 mM EGTA). Percentage of myogenic tone was used as a measure of myogenic responsiveness and was calculated at each intraluminal pressure as follows: % myogenic tone = $100*(D_0 - D)/D_0$, where D is external diameter under control conditions (Ca^{2+} PSS) or treated conditions (nifedipine, NNC 55–0396 or Ni^{2+}), and D_0 is external diameter in Ca^{2+}-free PSS. Percentage of maximal tone was used to ascertain the relative contribution of L- and T-type channels and was calculated at each intraluminal pressure as: % maximal tone = $100*\Delta D_X/D_0 - D$, where ΔD_X is change in arterial diameter induced by nifedipine or NNC 55–0396, D_0 is external diameter in Ca^{2+}-free PSS, and D is arterial diameter under control conditions (Ca^{2+} PSS).

Isolation of cerebral arterial smooth muscle cells

Smooth muscle cells from human, rat, or mouse cerebral arteries were enzymatically isolated as described previously (Harraz and Welsh, 2013). In brief, arterial segments (1–2-mm long) were placed in an isolation medium (at 37°C for 10 min) containing (mM): 60 NaCl, 80 Na-glutamate, 5 KCl, 2 $MgCl_2$, 10 glucose, and 10 HEPES with 1 mg/ml BSA, pH 7.4. Vessels were then exposed to a two-step digestion process that involved: (1) 10–15-min incubation in isolation medium (37°C) containing 0.5 mg/ml papain and 1.5 mg/ml dithioerythritol; and (2) a 15-min incubation in isolation medium containing 100 µM Ca^{2+}, 0.7 mg/ml of type F collagenase, and 0.3 mg/ml of type H collagenase. After incubation, tissues were washed repeatedly with ice-cold isolation medium and triturated with a fire-polished pipette. Isolated cells were kept in ice-cold isolation medium for use within ~6 h.

Quantitative PCR (qPCR)

Total RNA was isolated from human cerebral arteries or isolated smooth muscle cells using the RNeasy micro kit (QIAGEN) according to the manufacturer's recommendations. Control total RNA preparations from human whole brain or skeletal muscle were obtained from Takara Bio Inc., whereas human retina total RNA was provided by P. Schnetkamp (University of Calgary, Calgary, Canada). Reverse transcription was performed using the Quantitect reverse transcription kit (QIAGEN). For the negative control groups, all components except the reverse transcriptase were included in the reaction mixtures. Real-time PCR using intron-spanning primer sequences obtained from the qPrimer depot (Table S2; Cui et al., 2007) was performed using the Kapa SYBR Fast Universal qPCR kit (Kapa Biosystems). Human glyceraldehyde 3-phosphate dehydrogenase (GAPDH) gene was used as the reference gene. Control reactions and those containing cDNA from cerebral arteries were performed with 1 ng of template per reaction. Because of the limited quantities of RNA obtained from isolated smooth muscle cells (~200 cells), the entire cDNA yield from each preparation was used to assay the full set of test and housekeeping genes. The running protocol extended to 45 cycles consisting of 95°C for 5 s, 55°C for 10 s, and 72°C for 8 s using an Eppendorf Realplex 4 Mastercycler. PCR specificity was checked by dissociation curve analysis. Assay validation was confirmed by testing serial dilutions of pooled template cDNAs, suggesting a

linear dynamic range of 2.8–0.0028 ng of template and yielding percent efficiencies ranging from 80.4 to 108% (Table S3). No-template controls yielded no detectable fluorescence. Expression of the various Ca_V subtypes in human cerebral arteries or smooth muscle cells relative to whole brain ($Ca_V1.2$, $Ca_V1.3$, $Ca_V2.1$, $Ca_V2.2$, $Ca_V2.3$, $Ca_V3.1$, $Ca_V3.2$, and $Ca_V3.3$), skeletal muscle ($Ca_V1.1$), or retina ($Ca_V1.4$) was determined using the relative expression software tool (REST) version 2.0.13.

Western blot analysis

Whole human arteries were collected and frozen at −80°C in PBS, pH 7.4. The arteries were thawed on ice, centrifuged briefly to remove PBS, resuspended in low ionic strength buffer (10 mM Tris, pH 7.0, and 0.5 mM $MgCl_2$) containing Complete Ultra protease inhibitors (Roche), and incubated for 10 min on ice. The tissue was homogenized using a Polytron, followed by the addition of 1 volume solution A (0.5 M sucrose, 10 mM Tris, pH 7.0, 40 µM $CaCl_2$, 6 mM 2-mercaptoethanol, and 0.3 M KCl). After additional homogenization with the Polytron, the arteries were further subjected to 40 strokes in a Dounce homogenizer. The resulting crude lysate was centrifuged at 100,000 *g* for 1 h and resuspended in 50 µl of solution B (0.25 M sucrose, 10 mM Tris, pH 7.0, 20 µM $CaCl_2$, 3 mM 2-mercaptoethanol, and 0.15 M KCl). The protein concentration was determined with the Protein assay (Bio-Rad Laboratories) using BSA as the standard. The samples (4 µg per lane) were electrophoresed on a 5.6% polyacrylamide gel followed by transfer to PVDF membranes. The membranes were blocked for 1 h at room temperature using 0.2% Tropix I-Block (Applied Biosystems) in PBS followed by the addition of 1:200 diluted primary polyclonal antibodies raised against $Ca_V1.2$, $Ca_V3.2$, or $Ca_V3.3$ (Alomone Labs) overnight at 4°C. The membranes were washed three times for 10 min with PBS containing 0.1% Tween-20 followed by the addition of 1:10,000 goat anti–rabbit IRDye 800CW (Li-Cor Biosciences) for 1 h at room temperature, washed three times with PBS-Tween, and visualized using an infrared imaging system (Odyssey; Li-Cor Biosciences).

Electrophysiological recordings

Whole-cell currents were recorded using a patch-clamp amplifier (Axopatch 200B; Molecular Devices), filtered at 1 kHz, digitized at 5 kHz, and stored on a computer for offline analysis with Clampfit 10.3 software. Whole-cell capacitance was measured with the cancellation circuitry in the voltage-clamp amplifier. A 1-M NaCl–agar salt bridge between the reference electrode and the bath solution was used to minimize offset potentials (<2 mV). All electrophysiological recordings were performed at room temperature (∼22°C).

Ca_V channels. Conventional patch-clamp electrophysiology was used to monitor whole-cell Ca_V channel currents in isolated smooth muscle cells as reported previously (Harraz and Welsh, 2013). Recording electrodes (5–8 MΩ) were pulled from borosilicate glass microcapillary tubes (Sutter Instrument) using a micropipette puller (Narishige PP-830), and backfilled with pipette solution (mM): 135 CsCl, 5 Mg-ATP, 10 HEPES, and 10 EGTA, pH 7.2. Cells were voltage clamped and equilibrated in bath solution (mM): 110 NaCl, 1 CsCl, 10 $BaCl_2$, 1.2 $MgCl_2$, 10 glucose, and 10 HEPES, pH 7.4. For the experiment depicted in Fig. 3, bath solutions consisted of (mM): 110 NaCl, 1 CsCl, 1.2 $MgCl_2$, 10 glucose, and 10 HEPES plus charge carrier (1.8 Ca^{2+}, 1.8 or 10 Ba^{2+}). To record whole-cell currents, isolated smooth muscle cells were voltage clamped at a holding potential of −60 mV and subjected to a −90-mV prepulse (200 ms) and then to 10 voltage steps (300 ms) ranging from −50 to 40 mV (10-mV interval). I-V relationships were plotted as peak current (pA), current density (pA/pF), or normalized currents (I/I_{max}) at different voltage steps. For voltage ramp recordings, whole-cell currents were monitored using a voltage protocol that ramped from −100 to 100 mV (0.66 mV/ms). Voltage dependence of steady-state inactivation was assessed by a step protocol: (a) prepulse to −90 mV (300 ms); (b) stepping from −70 to +20 mV (10-mV intervals, 1.5 s each); (c) hyperpolarizing back to −90 mV (10 ms); and (d) stepping to a test voltage of 10 mV (200 ms). Whole-cell currents elicited by the test voltage were normalized to maximal current to plot $\%I/I_{max}$ versus voltage steps. Percentage of inactivation was calculated based on current amplitude at different time intervals (300, 600, 900, 1,200, and 1,500 ms) after peak current development. Inactivation time constants (τ) were obtained using Clampfit 10.3 software by standard exponential fitting of the inactivating segment of the current. To assess the voltage dependence of activation, isochronal tail currents were monitored. In particular, cells held at −60 mV were subjected to a prepulse (−90 mV, 300 ms), voltage steps (−80 to 40 mV, 10-mV intervals, 50 ms), and then a final hyperpolarizing test pulse (−90 mV, 200 ms) to evoke tail currents. Normalized tail currents ($\%I/I_{max}$) were plotted versus the voltage step. Activation time constants (τ) were obtained by standard exponential fitting of the activating downward segment of the whole-cell Ba^{2+} currents.

BK_{Ca} channels. Perforated patch-clamp electrophysiology was used to measure whole-cell K^+ currents in isolated human smooth muscle cells. The bath solution contained (mM): 134 NaCl, 4 KCl, 2 $MgCl_2$, 2 $CaCl_2$, 10 glucose, and 10 HEPES, pH 7.4. The pipette solution contained (mM): 110 K aspartate, 30 KCl, 10 NaCl, 2 $MgCl_2$, 10 HEPES, and 0.05 EGTA, pH 7.2, with 200 µg/ml amphotericin B. Membrane currents were gap-free recorded while the cells were voltage clamped at −40 mV. As reported previously (Harraz et al., 2014) and to analyze the frequency and amplitude of spontaneous transient outward K^+ currents (STOCs), the cutoff value was set to be three times the single-channel conductance.

Computational modeling

Network structure. A single complete arterial network of the cerebral vasculature was acquired using a micrograph of a resected brain biopsy. The micrograph was then manually segmented to obtain a network containing six orders (first–sixth) of branching arteries. This network was supplied by a single inflow vessel and contained 20 outflow vessels. To obtain a mathematical representation suitable for blood flow simulations, the network was discretized into 135 cylindrical vessel segments (213–1,700-mm long). Arterial diameter values were initially traced and set constant for each order according to average measured values (in µm): 600, 396, 261, 173, 114, and 75 for first, second, third, fourth, fifth, and sixth order vessels, respectively.

Blood flow. A previously developed theoretical model (Pries et al., 1990, 1994; Goldman and Popel, 2000) was used to calculate pressures and two-phase (erythrocyte and plasma) steady-state flows in the cerebral arterial network considered. This hemodynamic model implements conservation of blood volume flow (Q) and erythrocyte volume flow (QH_D) at each node joining two or three vessel segments, where H_D is the discharge (flow-averaged) hematocrit. These conservation equations are given below, where the sums are over all segments i connected to node j:

$$\sum_i Q_{ij} = 0 \quad \text{and} \quad \sum_i H_{Di} Q_{ij} = 0.$$

These equations are solved using the Poiseuille pressure–flow relation $\Delta P = 8\eta LQ/(R^4)$, where R and L are segment radius and length, respectively, and η is the blood viscosity. The model includes the following empirical properties of blood rheology:

(a) the Fahraeus effect, which determines how tube (volume-averaged) hematocrit varies with vessel diameter; (b) the Fahraeus–Lindqvist effect, which determines how viscosity varies with diameter and hematocrit; and (c) the phase separation (or plasma skimming) effect, which determines how erythrocytes are distributed at diverging bifurcations. The model requires specification of hematocrit at the inlet segment and specification of pressures at the upstream ends of the inlet segments and downstream ends of the outlet segments. All flow simulations used an inlet hematocrit of 0.42, and inlet and outlet pressures of 75 and 40 mmHg, respectively, in accordance with earlier studies that monitored the arterial pressure drop in cerebral vascular networks (Faraci and Heistad, 1990).

Myogenic tone and diameters. The pressure–diameter relationship measured in isolated human vessels under control conditions (see Fig. 1) was fit with a fourth-order polynomial, and this was used to adjust diameters from the initially constant values within each order given above based on the calculated pressures in each segment. Solutions were obtained iteratively, by alternating updates of pressures and flows with updates of diameters, until pressures, diameters, and flows became constant (steady state) throughout the model network. The same method was used for simulations in the presence of nifedipine, NNC, or Ni^{2+} (see Figs. 6 and 7), by using fourth-order polynomial fits to the measured variations in the pressure–diameter relationship.

Statistical analysis

Data are expressed as means ± SEM, and n = a/b indicates the number of vessels or cells (a) per the number of human subjects, rats, or mice (b). Where appropriate, paired or unpaired t tests, or one-way ANOVA was performed using SigmaPlot 12.5 to compare the effects of a given condition/treatment on arterial diameter, or whole-cell current. P-values ≤0.05 were considered statistically significant. Averaged I-V relationships were fit to the following Peak Gaussian third Parameter function: $I(V) = I_{max}*\exp[-0.5\{(V - V_{max})/b\}^2]$, where I_{max} is peak current (I), V_{max} is V at I_{max}, and b is the slope of the distribution. The voltage dependence of activation and steady-state inactivation were described with single Boltzmann distributions of the following forms: Activation: $I(V) = I_{max}/(1 + \exp[-(V - V_{50})/k])$; Inactivation: $I(V) = I_{max}/(1 + \exp[(V - V_{50})/k])$, where I_{max} is the maximal activatable current, V_{50} is the voltage at which the current is 50% activated or inactivated, and k is the slope of the distribution.

Online supplemental material

Fig. S1 reports low and high voltage-activated currents in human cerebral arterial smooth muscle, and that high millilmolar Ba^{2+} masks the separation of the two current components. Fig. S2 illustrates the effects of high concentrations of Ba^{2+} as the charge carrier on the I-V plots recorded in human smooth muscle. Fig. S3 depicts the biophysical properties of the nifedipine-sensitive and -insensitive currents in human cerebral arterial smooth muscle. Fig. S4 shows kinetic analysis of inward currents before and after the application of nifedipine. Fig. S5 compares representative traces and reversal potentials of Ba^{2+} currents recorded in human, mouse, and rat cerebral arterial smooth muscle cells. Table S1 reports the demographic characteristics of the origin of tissues and cells used. Tables S2 and S3 show the primer

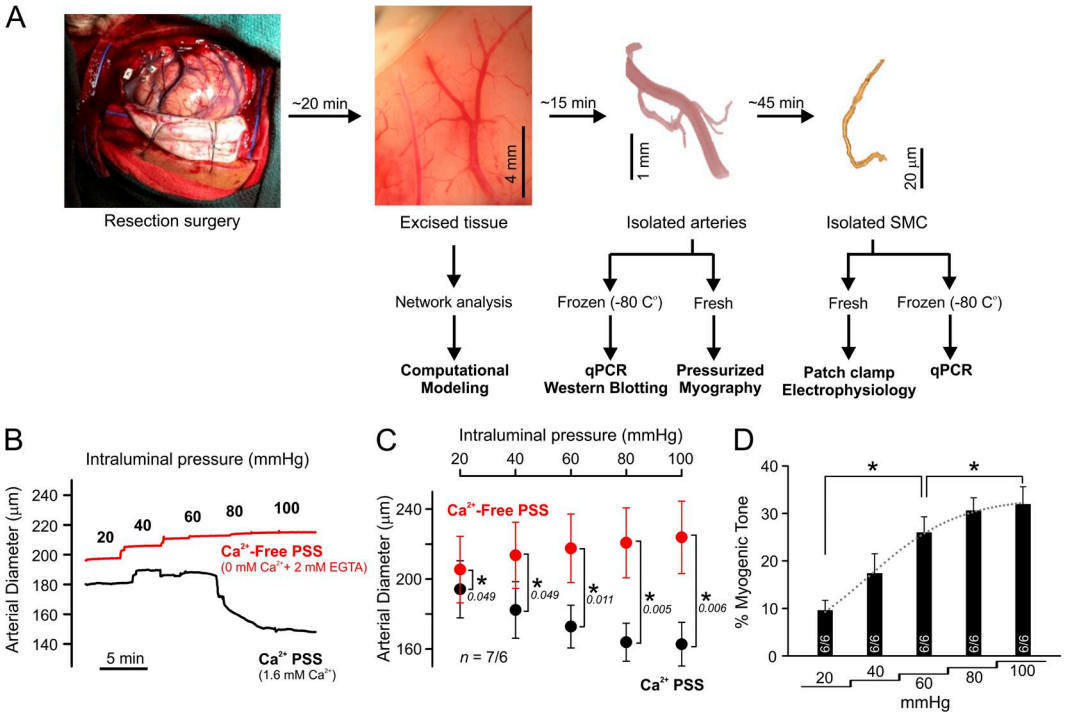

Figure 1. Human cerebral arteries exhibited myogenic activity. (A) Photomicrographs and timeline highlighting the general methodological procedures. (B and C) Representative traces and summary data illustrate that pressurized human cerebral arteries displayed myogenic activity whereby they constricted as intraluminal pressure sequentially increased from 20 to 100 mmHg in PSS. In Ca^{2+}-free PSS, cerebral arteries passively dilated (n = 7/6; three females; paired t test; *, P < 0.05; italic values denote probability). (D) Percentage of myogenic tone (see Materials and methods) was directly proportional to the applied intraluminal pressure (n = 6/6; three females; *, P < 0.05). Error bars denote SEM.

sequences and validation parameters for the qPCR analysis. The online supplemental material is available at http://www.jgp.org/cgi/content/full/jgp.201511361/DC1.

RESULTS

Human cerebral arteries exhibit myogenic activity

Pial cerebral arteries, isolated from patients undergoing brain resection surgery (Fig. 1 A and Table S1), were cannulated and mounted in a myograph and pressurized from 20 to 100 mmHg to assess myogenic reactivity. In physiological Ca^{2+} (1.6 mM), human cerebral arteries gradually constricted to increases in intraluminal pressure (Fig. 1, B and C); this active response was abolished by removing extracellular Ca^{2+} (0 mM Ca^{2+}/2 mM EGTA). Fig. 1 D illustrates that the percentage of myogenic tone increased progressively from 10% at 20 mmHg to 33% at 100 mmHg.

Human cerebral arterial smooth muscle expresses L- and T-type Ca^{2+} channels

Given the preceding Ca^{2+}-dependent observations, we screened for the α_1 pore–forming subunits of Ca_V channel subtypes ($Ca_V x.x$). Beginning with qPCR, analysis of human cerebral arteries and isolated smooth muscle cells revealed that all Ca_V subunits were expressed in the former, whereas only $Ca_V1.1$, $Ca_V1.2$, $Ca_V1.4$, $Ca_V3.2$, and $Ca_V3.3$ were expressed in the latter (Fig. 2 A). When standardized to reference tissue (whole brain: $Ca_V1.2$, $Ca_V1.3$, $Ca_V2.1$, $Ca_V2.2$, $Ca_V2.3$, $Ca_V3.1$, $Ca_V3.2$, and $Ca_V3.3$; skeletal muscle: $Ca_V1.1$; retina: $Ca_V1.4$), $Ca_V1.2$ and $Ca_V3.2$ were enriched in whole arteries (Fig. 2 B),

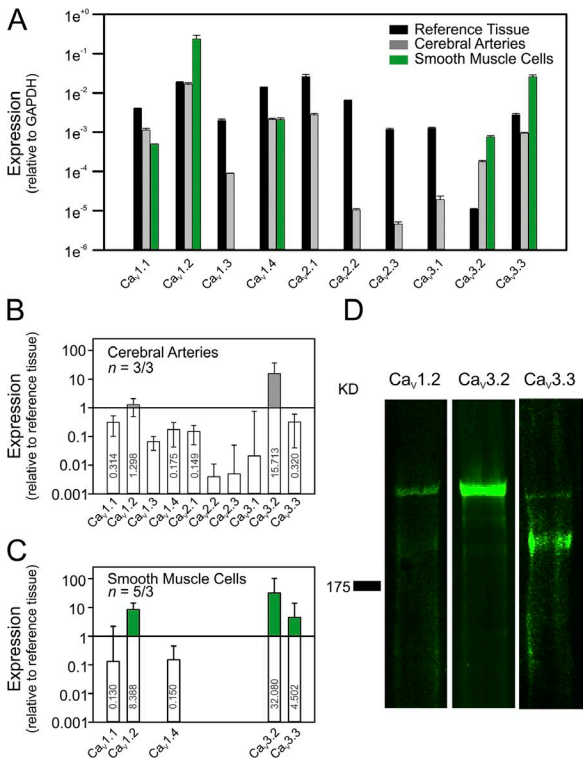

Figure 2. Human cerebral arteries express L- and T-type Ca^{2+} channels. (A) Screening mRNA for Ca_V channel subtypes ($Ca_V x.x$) in reference tissues, cerebral arteries (n = 3 PCR reactions on three groups of arteries from three patients; two females), or isolated smooth muscle cells (n = 5 PCR reactions on five digests of smooth muscle cells obtained from arteries of three patients; two females). qPCR was used to calculate the expression levels relative to the housekeeping gene human glyceraldehyde 3-phosphate dehydrogenase (GAPDH). (B and C) Expression of $Ca_V x.x$ mRNA in human cerebral arteries (B) or smooth muscle cells (C) was assessed relative to levels in reference tissues (whole brain: $Ca_V1.2$, $Ca_V1.3$, $Ca_V2.1$, $Ca_V2.2$, $Ca_V2.3$, $Ca_V3.1$, $Ca_V3.2$, and $Ca_V3.3$; skeletal muscle: $Ca_V1.1$; retina: $Ca_V1.4$). (D) Protein expression of the α_1 subunits of $Ca_V1.2$, $Ca_V3.2$, and $Ca_V3.3$ in human cerebral arteries was determined by Western blotting. Blots are representative of three independent experiments. Error bars denote SEM.

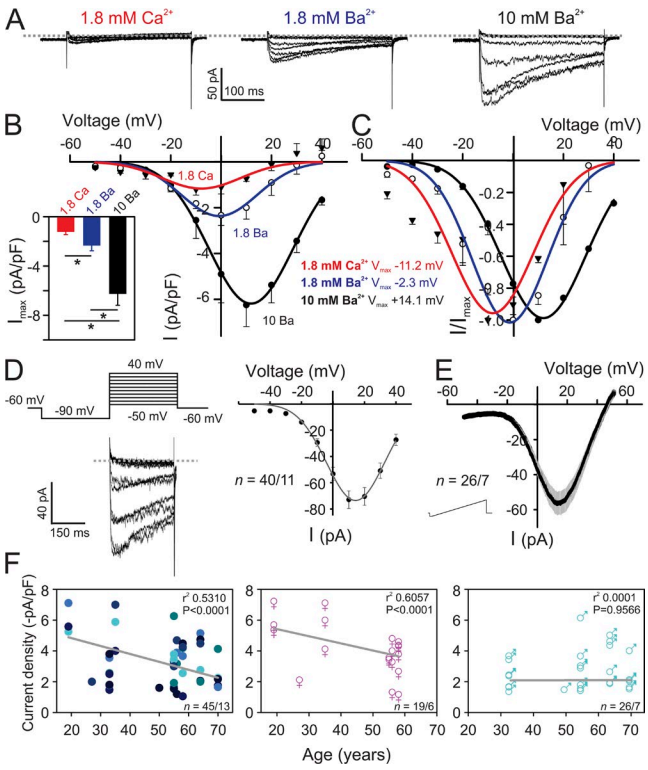

Figure 3. Ca_V channel currents in human cerebral arterial smooth muscle cells. (A) Representative traces of inward currents from one isolated cell under conditions in which 1.8 mM Ca^{2+} and 1.8 or 10 mM Ba^{2+} were alternatively used as the extracellular charge carrier. (B) Averaged effect (bar graphs and I-V plots) of the extracellular charge carrier on the amplitude of the inward current (n = 5/2; one female; *, $P < 0.05$). (C) Normalized I-V plots displayed a depolarizing shift upon changing from 1.8 mM Ca^{2+} to 1.8 mM Ba^{2+} and then 10 mM Ba^{2+}. (D) Representative trace and I-V plot of 10 mM Ba^{2+} currents (n = 40/11; five females) using the step protocol displayed. (E) Averaged I-V plots obtained using the ramp protocol (inset; n = 26/7; three females; gray denotes SEM). (F) Scatter plots of the correlation between current amplitude (pA/pF) and the age of the subjects from which cells were obtained. Left plot was obtained from 45 cells from 13 subjects (six females). Middle and right plots represent females (n = 19/6) and males (n = 26/7), respectively. Error bars denote SEM.

and $Ca_V1.2$, $Ca_V3.2$, and $Ca_V3.3$ displayed enriched expression in isolated smooth muscle cells (Fig. 2 C). Endothelial contamination of isolated smooth muscle samples was minimal as Von Willebrand factor mRNA levels decreased dramatically (~96%) compared with whole arteries. Focusing on the enriched targets, Western blot analysis confirmed the protein expression of $Ca_V1.2$, $Ca_V3.2$, and $Ca_V3.3$ in human cerebral arteries (Fig. 2 D).

Inward currents through human Ca_V channels

Using patch-clamp electrophysiology, we then monitored inward currents in cerebral arterial smooth muscle. Freshly isolated human cells were bathed in 1.8 mM Ca^{2+} and 1.8 or 10 mM Ba^{2+}; the first mimics physiological extracellular conditions, whereas the latter two accentuate charge flow through open Ca^{2+} channels. Stepping from −90 mV to voltage steps ranging from −50 to 40 mV, we observed a voltage-dependent inward current that was approximately fivefold less in 1.8 mM Ca^{2+} than in high [Ba^{2+}] (Fig. 3, A and B). Fig. 3 C illustrates the voltage dependence of the whole-cell currents, with normalized I-V plots showing that Ba^{2+} evoked a depolarizing shift compared with Ca^{2+}. Notably, normalized Ca^{2+} current (Fig. 3 C) exhibited a hyperpolarized threshold and an additional inward hump peaking at −30 mV, suggestive of a low voltage–activated current component (Fig. S1). The rightward shift associated with Ca^{2+} replacement could be further advanced by working with solutions containing 50 or 110 mM Ba^{2+} (Fig. S2). Given the small amplitude of native Ca^{2+} currents, subsequent recordings were performed in 10 mM Ba^{2+}; step and ramp voltage protocols elicited robust inward Ba^{2+} currents (Fig. 3, D and E). Linear regression analysis (Fig. 3 F) indicated an inverse correlation between peak current amplitude and age of subjects (r^2 = 0.531; P < 0.0001; age range 19–70 yr; n = 45/13; six females). This correlation was particularly evident in female (r^2 = 0.6057; P < 0.0001; 19–58 yr; n = 19/6) rather than male (r^2 = 0.0001; P = 0.9566; 33–70 yr; n = 26/7) subjects.

Delineating L- and T-type channels in human cerebral arterial smooth muscle

The whole-cell inward Ba^{2+} current depicted in Fig. 3 reflected simultaneous influx through L-type ($Ca_V1.2$) and T-type ($Ca_V3.2$/$Ca_V3.3$) Ca^{2+} channels. To effectively delineate between the two types, nifedipine was applied at a concentration (200 nM) that fully abolishes

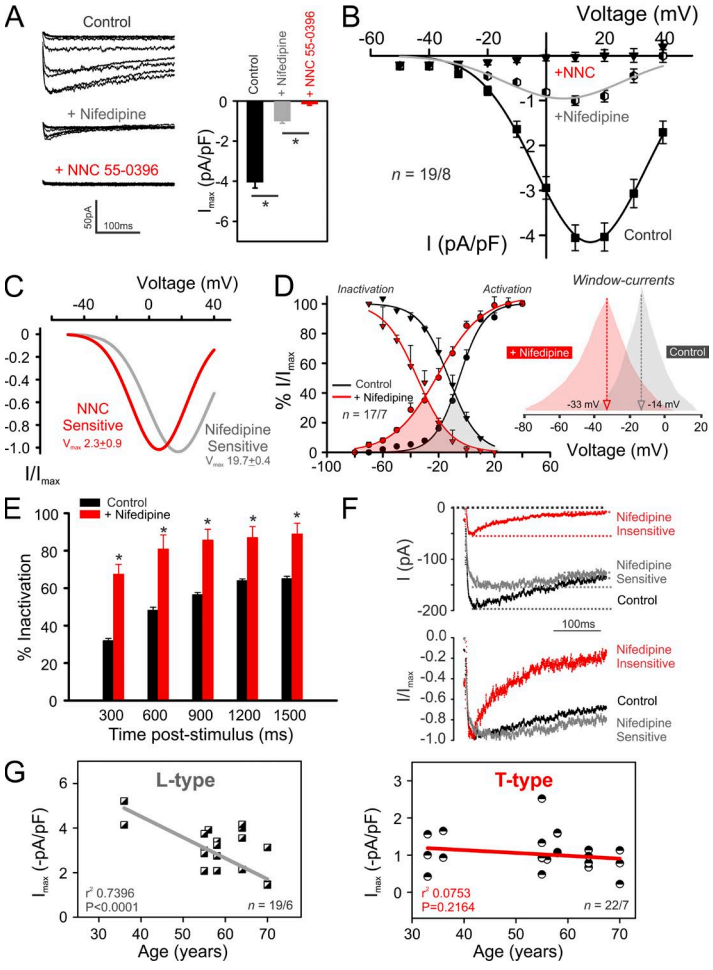

Figure 4. Electrophysiological delineation of L- and T-type channel currents in human arterial smooth muscle cells. (A) Representative and summary data depicting the cumulative effect of 200 nM nifedipine followed by 1 µM NNC 55–0396 on whole-cell Ba^{2+} currents (n = 19/8; four females; *, P < 0.05). (B) I-V-plots monitored under control conditions and after the application of nifedipine and then NNC 55–0396. (C) Normalized curve fits of the nifedipine-sensitive and NNC-sensitive subtracted currents. (D) Averaged effect of 200 nM nifedipine on the voltage dependence of activation and steady-state inactivation (n = 17/7; three females). Right inset highlights the shift in window currents. (E) Percentage of inactivation after a voltage step from −90 to 10 mV (n = 17/7; three females; paired t test; *, P < 0.05). (F) Representative kinetics of voltage-dependent inactivation of peak L- and T-type currents. The upper traces depict absolute amplitude (pA), and the lower traces represent normalized currents (I/I_{max}). (G) Scatter plots of the correlation between L- or T-type current density and the age of the subjects. Error bars denote SEM.

L- but not T-type currents (Liao et al., 2007; Harraz and Welsh, 2013); ∼75% block was observed (Fig. 4 A). Note that the use of different prepulse voltages was not successful in the separation of low and high voltage-activated Ca^{2+} channel currents in rodent cerebral arterial smooth muscle (Kuo et al., 2010; Abd El-Rahman et al., 2013). To test whether the residual nifedipine-insensitive current was dominated by a T-type conductance, we applied 1 µM NNC 55–0396. This T-type blocker abolished the remaining current, and I-V plots showed that nifedipine- and NNC-sensitive current components peaked (V_{max}) at 19.7 ± 0.4 mV and 2.3 ± 0.9 mV, respectively (Fig. 4, B and C). Caution is warranted when using pharmacological T-type blockers given their reported off-target effects on L-type channels (Kuo et al., 2010; Abd El-Rahman et al., 2013; Harraz and Welsh, 2013). Experiments in Fig. 4 (D–F) confirmed the successful delineation as nifedipine evoked hyperpolarized shifts in the voltage dependence of: (a) steady-state inactivation ($V_{50\text{-Inact}}$, −35.4 ± 2.3 mV vs. control, −12.7 ± 0.9 mV); (b) activation ($V_{50\text{-Act}}$, −20.3 ± 1.3 mV vs. control, −5.2 ± 0.8 mV); and (c) peak window current (−33.4 mV vs. control −14.1 mV). Kinetic analysis additionally noted that the nifedipine-insensitive T-type component inactivated faster (Fig. 4, E and F), exhibited rapid activation (T-type: τ_{Act}, 2.1 ms; L-type: τ_{Act}, 7.5 ms), and deactivated slower (T-type: τ_{Deact}, 8.9 ms; L-type: τ_{Deact}, 3.2 ms) compared with subtracted nifedipine-sensitive current (Fig. S3) or total control current (Fig. S4). Linear regression analysis (Fig. 4 G) indicated a negative correlation between age and the amplitude of the L-type ($r^2 = 0.7396$; $P < 0.0001$; 36–70 yr; $n = 19/6$) but not for T-type current ($r^2 = 0.0753$; $P = 0.2164$; 33–70 yr; $n = 22/7$).

Cross-species comparison of Ca_V channel activity

Past studies have shown that rat and mouse arterial smooth muscle express $Ca_V1.2$ (L), $Ca_V3.1$ (T), and $Ca_V3.2$ (T) subtypes (Kuo et al., 2010; Abd El-Rahman et al., 2013; Björling et al., 2013; Thuesen et al., 2014). Human cells displayed a similar expression profile, with the exception being that $Ca_V3.1$ was substituted by $Ca_V3.3$ (Fig. 2). Using patch-clamp electrophysiology, we compared the electrical properties of cerebral arterial Ca^{2+} channels between species using 10 mM Ba^{2+} as the charge carrier. Values of cell capacitance (pF), indicative of cell size, varied across species (Fig. 5 A). Inward current densities (pA/pF) were lower in human smooth muscle cells than in mouse or rat; however,

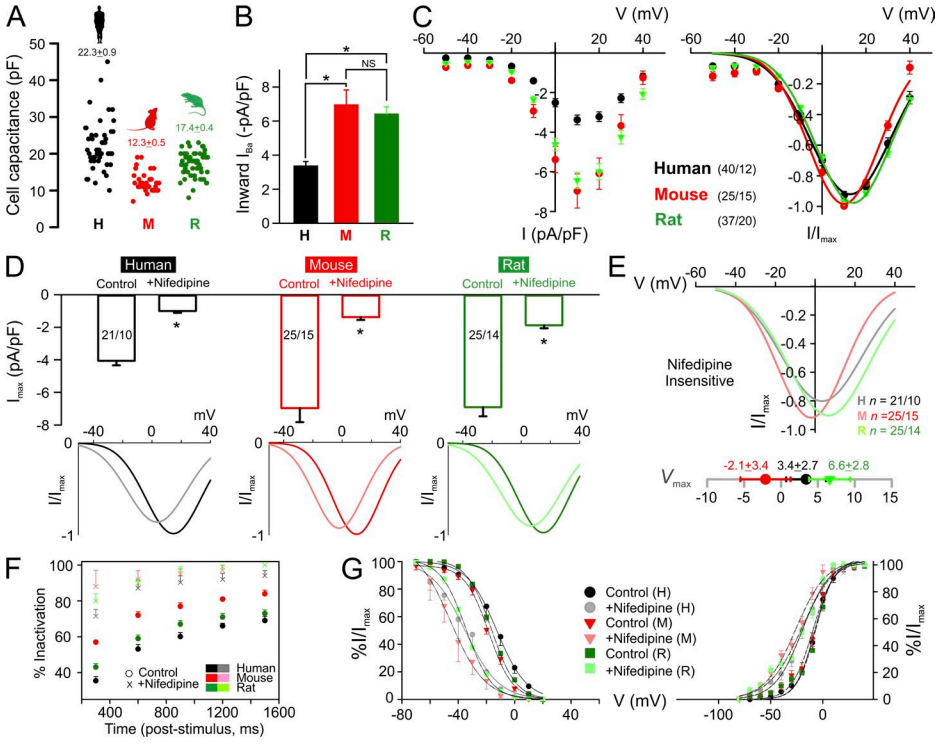

Figure 5. Electrophysiological comparison of Ca_V channels in cerebral arterial smooth muscle cells of humans, mice, and rats. (A) Scatter plot of cell capacitance (pF) obtained from human (H, black), mouse (M, red), or rat (R, green) cerebral arterial smooth muscle cells. (B) Amplitude of peak inward Ba^{2+} currents (*, $P < 0.05$; NS, not significant). (C) Absolute (pA/pF) and normalized I-V plots of inward currents (n = 40/12 human; six females; 25/15 mouse; 37/20 rat). (D) Bar graphs of current amplitude before (control) and after nifedipine (200 nM) treatment. Normalized plot fits (bottom) display the hyperpolarized shifts of T-type nifedipine-insensitive currents. *, $P < 0.05$, significant from respective control. (E) I-V plot fits of residual T-type currents. Bottom inset displays V_{max} values ($n = 21/10$ human; six females; 25/15 mouse; 25/14 rat). (F) Percentage of inactivation at different time points after a voltage step from −90 to 10 mV in the absence and presence of nifedipine. (G) Averaged effect of 200 nM nifedipine on voltage dependence of steady-state inactivation (left) and activation (right); average normalized data (%I/I_{max}) were fit with single Boltzmann distributions. Error bars denote SEM.

normalized currents displayed comparable dependence on voltage (Fig. 5, B and C). Whole-cell currents inactivated faster in mouse smooth muscle cells, whereas the reversal potential of rat currents was depolarized relative to human or mouse (Fig. S5). 200 nM nifedipine elicited comparable blockade across species, and the residual insensitive currents displayed 10–20-mV hyperpolarized shifts consistent with T-type activity (Fig. 5, D and E). In all three species, L-type channel inhibition quickened inactivation and leftward shifted the activation/inactivation profiles (Fig. 5, F and G).

L- and T-type Ca^{2+} channels contribute to human myogenic tone development

In rodent cerebral arteries, studies have shown that L- and T-type channels ($Ca_V1.2$ and $Ca_V3.1$) facilitate myogenic tone development at high and low intraluminal pressures, respectively (Abd El-Rahman et al., 2013; Björling et al., 2013). Both conductance types (L-type: $Ca_V1.2$; T-type: $Ca_V3.3$ substituting for $Ca_V3.1$) are present in human cerebral arteries and, as such, comparable experiments were conducted on pressurized human vessels to elucidate potential roles of Ca^{2+} channels. Similar to electrophysiology, L-type Ca^{2+} channel blockade preceded T-type suppression to minimize off-target effects. 200 nM nifedipine induced a vasodilator response in human vessels that was limited at low pressure and maximal at 80–100 mmHg. The additional application of a T-type blocker (1 µM NNC 55–0396) modestly dilated arteries in a pressure-dependent manner, with peak responses at 40–60 mmHg (Fig. 6, A–C). Data in Fig. 6 (B and C) displayed distinctive L- and T-type vasomotor trends, although statistical significance was not achieved because of limited observations ($n = 3/3$; $P = 0.087–0.157$). As such, the relative contribution of the two conductances to developed myogenic tone was dynamic, with T-type channels ($Ca_V3.3$) prevailing at lower pressures when the V_M was relatively hyperpolarized and L-type channels ($Ca_V1.2$) dominating at higher pressures when smooth muscle is strongly depolarized (Fig. 6 D).

$Ca_V3.2$ channels and BK_{Ca}-mediated STOC activity

To discriminate between the contributions of $Ca_V3.2$ and $Ca_V3.3$ to myogenic constriction, we examined the effects of a specific $Ca_V3.2$ blocker (50 µM Ni^{2+}) on isolated human smooth muscle cells and arteries. At this concentration, Ni^{2+} was verified to selectively suppress $Ca_V3.2$ currents, but not other L- or T-type channels expressed in arterial smooth muscle or expression systems (Lee et al., 1999; Harraz and Welsh, 2013; Harraz et al., 2014). Starting with electrophysiology, we confirmed that 50 µM Ni^{2+} partially suppressed the nifedipine-insensitive $Ca_V3.x$ current (Fig. 7, A and B). A kinetic analysis followed, and time constant measurements revealed that the Ni^{2+}-sensitive current activated and inactivated faster ($Ca_V3.2$: τ_{Act}, 0.9 ± 0.1 ms; τ_{Inact}, 17.1 ± 3.3 ms) than the insensitive current ($Ca_V3.3$: τ_{Act}, 4.3 ± 0.3 ms; τ_{Inact}, 48.7 ± 9.5 ms), consistent with Ni^{2+} selectively blocking $Ca_V3.2$ (Fig. 7, C and D) (Lee et al., 1999; Perez-Reyes, 2003). We next applied 50 µM Ni^{2+} onto pressurized human arteries, and contrary to the vasodilation observed with a broad spectrum T-type blocker (NNC 55–0396; Fig. 6), Ni^{2+} enhanced myogenic constriction at pressures ≤60 mmHg (Fig. 7, E and F). Interestingly, Ni^{2+}- and NNC 55–0396-induced vasomotor changes were pressure dependent but modestly different from one another, a finding that aligns with the voltage profiles of $Ca_V3.2$ and $Ca_V3.3$ (Fig. 7 G). The

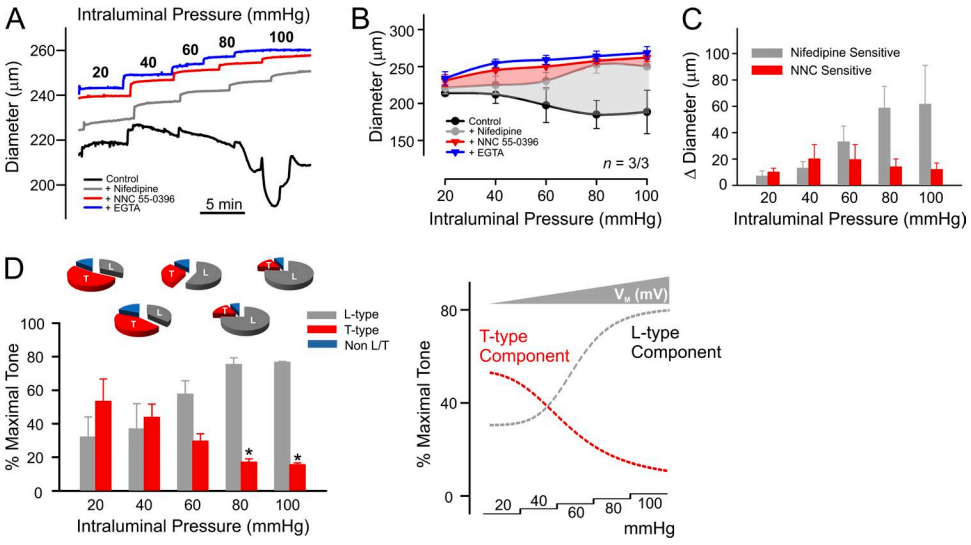

Figure 6. L- and T-type Ca^{2+} channels contribute to human arterial myogenic tone in a pressure-dependent manner. (A and B) Representative traces and summary data showing that human arteries displayed prominent myogenic activity under control conditions (black). Consecutive pharmacological suppression of L-type (200 nM nifedipine) and T-type (1 µM NNC 55–0396) channels dilated pressurized human cerebral arteries ($n = 3/3$; one female). (C) Absolute changes in diameter (µm) in response to nifedipine or NNC 55–0396 at intraluminal pressures from 20 to 100 mmHg. (D) Percentage of contribution of the L-type channel (gray) to maximal arterial tone was directly proportional to intraluminal pressure. In contrast, the T-type contribution (red) was inversely proportional and significantly different from that of L-type at 80 and 100 mmHg. Percentage of the maximal tone was mathematically calculated from three independent experiments ($n = 3/3$; one female; *, $P < 0.05$). Right inset represents fits of L- versus T-type components of maximal tone within a range of pressure steps (mmHg). Error bars denote SEM.

preceding Ni^{2+} observations suggest, in accordance with rat studies (Harraz et al., 2014), that $Ca_V3.2$ mediates a negative feedback response by downstream triggering of BK_{Ca} channels to initiate STOCs. Perforated patch-clamp electrophysiology indicated the presence of STOCs in human smooth muscle cells and showed that 50 µM Ni^{2+} significantly reduced the frequency (control, 1.30 ± 0.35 Hz; Ni^{2+}, 0.69 ± 0.17 Hz) but not the amplitude (control, 6.87 ± 0.09 pA; Ni^{2+}, 6.56 ± 0.25 pA) of these events (Fig. 7 H).

Predicted changes in cerebral blood flow by Ca^{2+} channel modulators

Myography experiments (Figs. 6 and 7) showed that human cerebral arterial Ca^{2+} channel subtypes elicited divergent vasomotor effects whereby $Ca_V1.2/Ca_V3.3$ augmented but $Ca_V3.2$ counterbalanced myogenic constriction. To conceptually ascertain how each channel subtype could influence cerebral blood flow, a computational model was developed using an arterial network map (lengths and basal diameters) generated from a photomicrograph of excised human brain tissue (see Materials and methods; Fig. 8, A–C). Intraluminal pressure within the virtual model varied, with inlet and outlet pressures set to 75 and 40 mmHg, respectively (Faraci and Heistad, 1990). The pressure–diameter relationship measured in isolated human vessels in the absence and presence of nifedipine, NNC 55–0936, or Ni^{2+} was fit with a fourth-order polynomial, and these percentage values were used to adjust the initially constant diameters within each segment (Fig. 8 D). This integration enabled the calculation of steady-state distributions of pressure, diameter, and blood flow for each arterial segment (135 in total; Fig. 8 E). Two-dimensional plots and color-coded virtual networks indicated that the suppression of $Ca_V1.2$ and to a lesser extent $Ca_V3.3$ increased network blood flow in a pressure/diameter-dependent manner. In contrast, $Ca_V3.2$ inhibition constricted arterial segments and decreased cerebral blood flow (Fig. 8 F).

DISCUSSION

This study delineated Ca_V channels in human cerebral arteries and determined subtype-specific contributions to arterial tone development. Experiments progressed from cells to tissues and used pressurized myography,

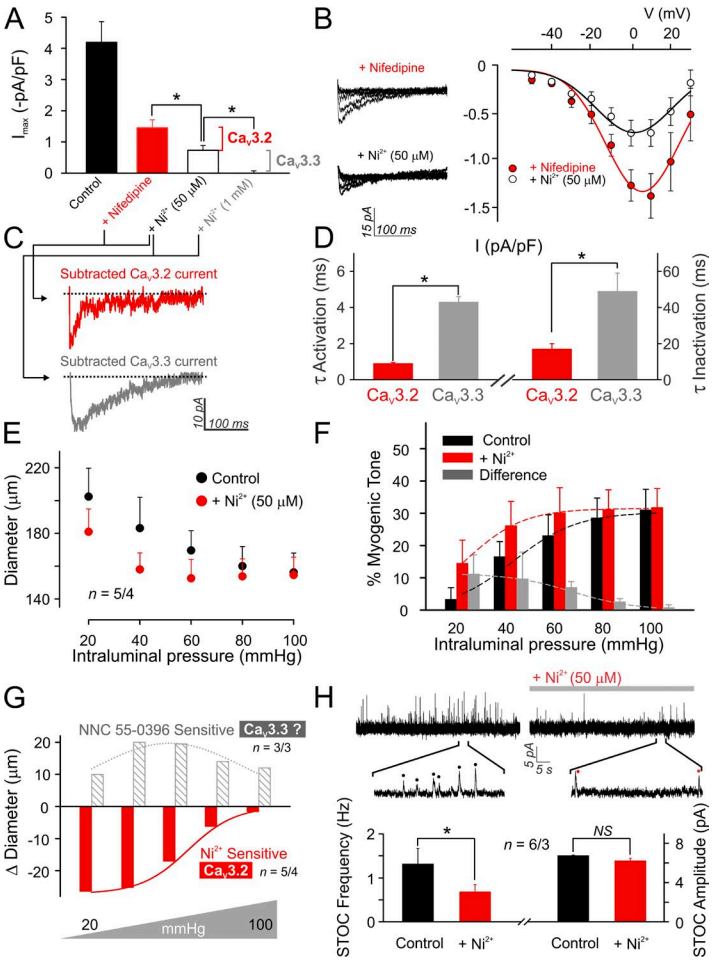

Figure 7. Delineation of $Ca_V3.2$ channel activity and function. (A) Bar graph illustrates that 50 µM Ni^{2+} ($Ca_V3.2$ blocker) suppresses nifedipine-insensitive T-type currents. Subsequent application of 1 mM Ni^{2+} abolished residual Ba^{2+} currents ($n = 6/5$; three females; *, $P < 0.05$). (B) Representative traces and averaged plots show that T-type current ($Ca_V3.2 + Ca_V3.3$) was 50% suppressed by 50 µM Ni^{2+}. (C and D) Traces and activation/inactivation time constants (τ) of subtracted $Ca_V3.2$ and $Ca_V3.3$ currents. $Ca_V3.2$ currents exhibited faster activation and inactivation kinetics compared with $Ca_V3.3$ currents ($n = 5/4$; two females; paired t test; *, $P < 0.05$). (E and F) $Ca_V3.2$ blockade (50 µM Ni^{2+}) constricted pressurized human cerebral arteries and augmented myogenic tone most prominently at lower pressure values (20–60 mmHg, $n = 5/4$; two females). (G) Averaged changes in arterial diameters after application of the nonselective T-type blocker (1 µM NNC 55–0396; $n = 3/3$; one female; gray) or the selective $Ca_V3.2$ blocker (50 µM Ni^{2+}; $n = 5/4$; two females; red). Error bars were excluded for clarity of presentation. Curve fits highlight the differential pressure/voltage dependence of a $Ca_V3.3$ (gray) versus a $Ca_V3.2$ (red) component. (H) Representative traces (top) and summary data (bottom) illustrating the effect of 50 µM Ni^{2+} on STOC frequency and amplitude. All recordings were obtained while cells were held at −40 mV ($n = 6/3$; one female; paired t test; *, $P < 0.05$). Error bars denote SEM.

PCR, Western blotting, electrophysiology, and computational modeling. Messenger RNA and protein analyses revealed the expression of L- and T-type α_1 pore–forming subunits in cerebral arterial smooth muscle. Patch-clamp recordings subsequently confirmed the presence of inward current divisible into L- and T-type components in isolated human smooth muscle cells. In pressurized human arteries, L- ($Ca_V1.2$) and T-type ($Ca_V3.3$) channel suppression dilated arteries in a pressure-dependent manner at higher and lower intraluminal pressures, respectively. Subtype-specific targeting of $Ca_V3.2$ paradoxically implicated this conductance in restraining arterial constriction via a mechanism involving BK_{Ca} channels. In a final set of experiments, computational modeling conceptually illustrated how each Ca_V subtype plays a distinctive role in setting cerebral blood flow. To summarize, this study reports for the first time the expression and divergent functions of three Ca^{2+} channel subtypes in human cerebral arteries.

A century ago, Bayliss (1902) first described the inherent ability of resistance arteries to constrict to elevated arterial pressure, a phenomenon known as the myogenic response. In the cerebral circulation, this myogenic response is essential to maintain brain perfusion, and a global rise in smooth muscle $[Ca^{2+}]_i$ is critical to the transduction process. Like most stimuli, elevated intraluminal pressure drives a rise in cytosolic $[Ca^{2+}]_i$ through the induction of arterial depolarization and subsequent activation of voltage-gated L-type $Ca_V1.2$ channels (Knot and Nelson, 1998). Although a dominant player, animal studies have noted other Ca^{2+} channels (T-type, $Ca_V3.1/Ca_V3.2$) in cerebral arteries (Kuo et al., 2010; Abd El-Rahman et al., 2013). Distinct from the "long-lasting" kinetics and high voltage activation profile of the "L"-type conductance, "T"-type channels are characteristically "transient" and activate at more hyperpolarized voltages (Perez-Reyes, 2003; Catterall, 2011). Although Ca^{2+} entry events through L-type channels ($Ca_V1.2$ sparklets) have been characterized in vascular smooth muscle (Navedo et al., 2005), $Ca_V3.x$ sparklets remain to be investigated. They would likely display spatiotemporal characteristics distinct from $Ca_V1.2$ and which according to their single-channel properties would be more transient in nature and smaller in magnitude (Perez-Reyes, 2003). Recent studies in rodents have implied that T-type channels modulate myogenic tone, albeit in a manner unique and sometimes paradoxical to L-type channels (Chen et al., 2003; Kuo et al., 2010; Abd El-Rahman et al., 2013; Björling et al., 2013; Harraz et al., 2014). Despite the growing interest and therapeutic potential, human studies to date have failed to establish whether T-type channels are present in key vascular beds and if so, how they influence arterial tone.

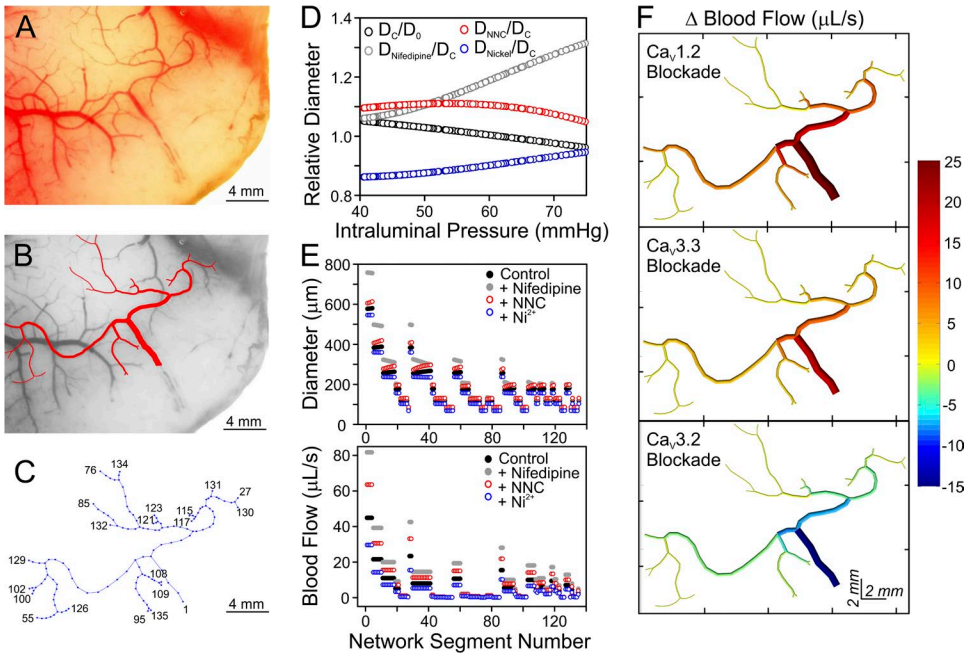

Figure 8. Predicted influence of L- and T-type Ca^{2+} channels on blood flow in human cerebral arteries. (A and B) A photomicrograph of excised human brain tissue was used to generate an arterial network of defined dimensions. (C) The segmented network was skeletonized into vessel segments producing a mathematical representation useful for blood flow simulations; 1 marks the first inflow segment, and the other numbered boundary segments are outflows. Inlet and outlet pressures were set to 75 and 40 mmHg, respectively. (D and E) Using myography data, we modeled the vasomotor behavior of virtual arterial segments across a range of pressures (40–75 mmHg), in the absence and presence of nifedipine, NNC 55–0936, or Ni^{2+}. Responses were incorporated into the model and steady-state distributions of diameter; pressure and blood flow were calculated for each arterial segment. (F) Color-coded maps of changes in blood flow illustrate the effects of $Ca_V1.2$, $Ca_V3.3$, or $Ca_V3.2$ channels on network perfusion.

Within this context, we began to isolate human cerebral arteries from patients undergoing resection surgery. Using vessel myography, we observed for the first time that human cerebral arteries constrict robustly to an increase in intraluminal pressure, with percentages of myogenic responses aligning with previous animal studies (Knot and Nelson, 1998; Cole and Welsh, 2011). The removal of extracellular Ca^{2+} abolished myogenic constriction, an observation consistent with elevated pressure evoking Ca^{2+} flux through Ca_V channels (Knot and Nelson, 1998). 10 genes encode for the α_1 pore–forming subunits of Ca^{2+} channels (Catterall, 2011), and molecular analyses showed robust mRNA expression of three subtypes (Fig. 2). $Ca_V1.2$ (L-type) and $Ca_V3.2$ (T-type) were present in isolated human smooth muscle cells prescreened for endothelial contamination. Messenger RNA of $Ca_V3.3$ was also observed while $Ca_V3.1$ was minimally expressed, a finding distinct from rodents (Kuo et al., 2010; Abd El-Rahman et al., 2013; Björling et al., 2013). Compared with $Ca_V3.1$, $Ca_V3.3$ channel displays slower activation/inactivation kinetics and activates at relatively depolarized potentials (Monteil et al., 2000; Frazier et al., 2001; Chemin et al., 2002). One could rationalize, in this regard, that $Ca_V3.3$ may be better suited than $Ca_V3.1$ to drive cellular functions requiring sustained Ca^{2+} flux (Chemin et al., 2002), such as smooth muscle contraction and arterial tone development. Western blot analysis confirmed protein expression of all three subtypes in whole arteries.

Having detected their message and protein expression, electrophysiological recordings followed to separate L- and T-type conductances in human cerebral arterial smooth muscle. Human cells demonstrated a small inward current in physiological Ca^{2+} solutions that displayed a voltage-dependent I-V profile consistent with Ca^{2+} channel activation (Fig. 3). Exchange of physiological Ca^{2+} for higher millimolar Ba^{2+} dramatically enhanced inward current, masked the low voltage–activated Ca^{2+} current component, and induced a depolarized shift in the voltage profile without destabilizing the cell. The latter shift is presumably responsible for masking the hyperpolarized current component and is reflective of a high divalent cation screening effect and barium's preferential permeability through L-type channels (Perez-Reyes, 2003; Li et al., 2010). Using nifedipine at concentrations that fully block the smooth muscle splice variant of L-type $Ca_V1.2$ channels (Liao et al., 2007; Harraz and Welsh, 2013), a partial suppression of Ba^{2+} currents occurred. Note that nifedipine has been shown to lack an effect on $Ca_V3.x$ in vascular smooth muscle or expression systems when applied in the submicromolar ranges (Harraz and Welsh, 2013; Harraz et al., 2014). Three lines of evidence subsequently confirmed that L- and T-type channels, respectively, carried the nifedipine-sensitive and -insensitive components. First, the nifedipine-insensitive current was actively blocked by T-type inhibitors. Second, the presumed L- and T-type currents displayed depolarized and hyperpolarized profiles, respectively, in accordance with conductances being high and low voltage activated. Third, the residual insensitive conductance activated and inactivated faster, in keeping with the transient nature of T-type channels (Catterall, 2011). $Ca_V3.x$ currents recorded in human arterial smooth muscle display kinetics similar to those in heterologous expression systems. Note, however, they do display a depolarized voltage-dependent profile because of the use of high millimolar Ba^{2+} as the permeant recording ion (Perez-Reyes, 2003; Harraz and Welsh, 2013). Overall, these findings are unique in the vascular literature and are the first to show that multiple Ca_V conductances are not only present but also electrically active in native human arterial smooth muscle.

Despite their diverse demographic origins, Ca^{2+} channel currents were resolved in all tested cells. With that said, an intriguing inverse relationship between current amplitude and donor age existed (Fig. 3), similar to reports in animal models (Georgeon-Chartier et al., 2013; Fukuda et al., 2014). This relationship was sexually dimorphic and manifested exclusively in females. These observations suggest that Ca^{2+} channel expression and/or activity may be under the regulation of sex hormones (Bowles et al., 2004; Ullrich et al., 2007); however, caution is warranted given the limited sample size and the pathological state of the human subjects. Further analysis showed that the preceding age–current correlation stemmed primarily from variations in L-type activity (Fig. 4), a finding that indicates that the efficacy of calcium channel blockers in the treatment of constrictive disorders may be altered or compromised in the elderly (Kumar and Hall, 2003; Fukuda et al., 2014).

Recent rodent studies have suggested that both L- and T-type channels play a direct role in elevating cytosolic $[Ca^{2+}]_i$ and myogenic tone, albeit at specific V_Ms (Abd El-Rahman et al., 2013; Björling et al., 2013). In particular, the L-type $Ca_V1.2$ channels appear to dominate at elevated pressures when vessels are depolarized. In comparison, the low voltage–activated T-type $Ca_V3.1$ channels are thought to facilitate tone development at lower pressures when smooth muscle resides in a hyperpolarized state (Abd El-Rahman et al., 2013; Björling et al., 2013). Human L- and T-type channels could operate similarly, and to pursue this hypothesis, a two-step approach was instituted. Starting with a comparative electrical analysis, findings in Fig. 5 illustrate that human, rat, and mouse smooth muscle cells all exhibited L- and T-type current components, with human cells displaying smaller amplitudes. No substantive difference was observed in activation/steady-state inactivation voltage profiles, although inactivation kinetics were faster in mouse smooth muscle. Given these similarities, we next pressurized human cerebral arteries from 20 to

100 mmHg and performed vessel myography under control conditions and in the presence of L-type (nifedipine) and T-type (NNC 55–0396) channel blockers. In a pressure-dependent manner, L- and T-type blockers evoked vasodilation in myogenically responsive arteries (Fig. 6). L- and T-type channels dominated myogenic tone at higher and lower pressures, respectively, in accordance with the physiological window currents of $Ca_V1.2$ and $Ca_V3.x$ channels. Reduced Ca^{2+} flux through $Ca_V3.3$ channels is most likely responsible for the vasodilator response to NNC 55–0396, as findings below note that selective $Ca_V3.2$ blockade induces arterial constriction. Our observations are the first to invoke a role for T-type channels in human cerebral arteries, and arguably this conductance may dominate Ca^{2+} entry in distal arteries where intraluminal pressures are ∼30–45% less than systemic (Faraci and Heistad, 1990). If true, it follows that constrictive disorders in smaller arteries may be more effectively treated by simultaneous L- and T-type channel suppression, a view consistent with clinical findings (Beltrame et al., 2004; Ogura et al., 2012; Sugano et al., 2013).

Studying T-type channels in native cells has been consistently limited by the lack of subtype-specific modulators. One exception is Ni^{2+}, a divalent cation that preferentially blocks $Ca_V3.2$ channels when applied in the low micromolar range (Lee et al., 1999; Harraz et al., 2014). In rat cerebral arterial smooth muscle and HEK cells, Ni^{2+} abolished $Ca_V3.2$, but not other high or low voltage–activated Ca^{2+} currents. Previous experiments have additionally shown that Ni^{2+} lacked any effects on cells and arteries where $Ca_V3.2$ channels had been genetically ablated (Harraz and Welsh, 2013; Harraz et al., 2014). Exploiting this tool, electrophysiological experiments followed by kinetic analysis confirmed that 50 µM Ni^{2+} inhibited $Ca_V3.2$ but not $Ca_V3.3$ channels in human cerebral arterial smooth muscle cells. In paradoxical contrast to the vasodilation induced by a broad-spectrum T-type blocker, Ni^{2+} enhanced myogenic constriction at pressures ≤60 mmHg (Fig. 7). Such results suggest a distinctive role of $Ca_V3.2$ channels, perhaps involving a vasodilator conductance sensitive to Ca^{2+} and/or voltage. In this regard, recent rodent literature has argued that $Ca_V3.2$ can trigger Ca^{2+} release from the sarcoplasmic reticulum in the form of Ca^{2+} sparks, and that the subsequent generation of Ca^{2+} sparks elicits hyperpolarization via BK_{Ca} channels (Chen et al., 2003; Harraz et al., 2014). To address this possibility, we monitored BK_{Ca}-mediated STOC activity in human cells, and in support of our hypothesis, Ni^{2+} inhibited these transient hyperpolarizing currents. It is worth noting that previous whole-cell and whole arterial recordings argued against a direct modulatory role of Ni^{2+} on K^+ channels when applied at low micromolar concentrations (Harraz et al., 2014). Our findings challenge the stereotypic view that Ca^{2+} channels only facilitate myogenic constriction. They further highlight the view that if T-type modulators are to be used therapeutically to treat cardiovascular disorders (Giordanetto et al., 2011), subtype specificity should be thoughtfully considered.

With $Ca_V1.2$, $Ca_V3.2$, and $Ca_V3.3$ channels distinctively influencing arterial diameter, logic dictates that unique blood flow responses should ensue. Although it is impractical to monitor cerebral blood flow in small human arteries, such responses can be predicted in a virtual arterial network (Pries et al., 1990, 1994; Goldman and Popel, 2000). Using architectural and vasomotor data from human arteries, we consequently designed a computational model that mimics a native arterial network. Findings in Fig. 8 highlight that $Ca_V1.2$ or $Ca_V3.3$ inhibition dilated virtual cerebral arteries and increased network blood flow. $Ca_V1.2$ blockade elicited a particularly profound response in larger arteries, vessels that harbor higher intraluminal pressures. Subtype-specific suppression of $Ca_V3.2$ alternatively constricted arterial segments, diminishing network cerebral blood flow. Such predictions conceptually emphasize the differential significance of Ca^{2+} channels in matching blood flow with brain metabolic activity.

This study identified Ca_V channels in human cerebral arteries and ascertained how each conductance influences myogenic tone. Molecular and electrophysiological analyses demonstrated that α_1 subunits of L- ($Ca_V1.2$) and T-type ($Ca_V3.2$ and $Ca_V3.3$) channels are robustly expressed in human cerebral arterial smooth muscle. In myogenically active human arteries, $Ca_V1.2$ inhibition induced vasodilation at high intraluminal pressures, whereas $Ca_V3.3$ blockade induced modest dilation at lower pressures when vessels resided in a hyperpolarized state. Paradoxically, cerebral arterial $Ca_V3.2$ channels appear to attenuate myogenic tone through the downstream activation of BK_{Ca} channels.

We thank Dr. Bjorn Hald, Dr. Christophe Altier, and Dr. Michael Walsh for critical comments on the preliminary figures.

This work was supported by an operating grant from the Canadian Institutes of Health Research (CIHR; MOP-69088 to D.G. Welsh). D.G. Welsh is an Alberta Innovates-Health Solutions (AIHS) senior scholar and holds a Canada Research Chair. O.F. Harraz is a Vanier Scholar (CIHR) and was supported by salary studentships from AIHS and Achievers in Medical Sciences (AIMS scholarship). D. Goldman was partially supported by a Discovery grant from the Natural Sciences and Engineering Research Council of Canada (NSERC, R4081A03). A. Zechariah was supported by AIHS and Eyes High postdoctoral fellowships. A.M. Hashad was a Vanier Scholar and a recipient of an AIHS studentship.

The authors declare no competing financial interests.

Richard L. Moss served as editor.

Submitted: 13 January 2015
Accepted: 16 March 2015

REFERENCES

Abd El-Rahman, R.R., O.F. Harraz, S.E. Brett, Y. Anfinogenova, R.E. Mufti, D. Goldman, and D.G. Welsh. 2013. Identification of L- and T-type Ca^{2+} channels in rat cerebral arteries: role in myogenic tone development. *Am. J. Physiol. Heart Circ. Physiol.* 304:H58–H71. http://dx.doi.org/10.1152/ajpheart.00476.2012

Bayliss, W.M. 1902. On the local reactions of the arterial wall to changes of internal pressure. *J. Physiol.* 28:220–231. http://dx.doi.org/10.1113/jphysiol.1902.sp000911

Beltrame, J.F., S.P. Turner, S.L. Leslie, P. Solomon, S.B. Freedman, and J.D. Horowitz. 2004. The angiographic and clinical benefits of mibefradil in the coronary slow flow phenomenon. *J. Am. Coll. Cardiol.* 44:57–62. http://dx.doi.org/10.1016/j.jacc.2004.03.055

Björling, K., H. Morita, M.F. Olsen, A. Prodan, P.B. Hansen, P. Lory, N.H. Holstein-Rathlou, and L.J. Jensen. 2013. Myogenic tone is impaired at low arterial pressure in mice deficient in the low-voltage-activated CaV 3.1 T-type $Ca^{(2+)}$ channel. *Acta Physiol. (Oxf.).* 207:709–720. http://dx.doi.org/10.1111/apha.12066

Bowles, D.K., K.K. Maddali, V.K. Ganjam, L.J. Rubin, D.L. Tharp, J.R. Turk, and C.L. Heaps. 2004. Endogenous testosterone increases L-type Ca^{2+} channel expression in porcine coronary smooth muscle. *Am. J. Physiol. Heart Circ. Physiol.* 287:H2091–H2098. http://dx.doi.org/10.1152/ajpheart.00258.2004

Catterall, W.A. 2011. Voltage-gated calcium channels. *Cold Spring Harb. Perspect. Biol.* 3:a003947. http://dx.doi.org/10.1101/cshperspect.a003947

Chemin, J., A. Monteil, E. Perez-Reyes, E. Bourinet, J. Nargeot, and P. Lory. 2002. Specific contribution of human T-type calcium channel isotypes (alpha(1G), alpha(1H) and alpha(1I)) to neuronal excitability. *J. Physiol.* 540:3–14. http://dx.doi.org/10.1113/jphysiol.2001.013269

Chen, C.C., K.G. Lamping, D.W. Nuno, R. Barresi, S.J. Prouty, J.L. Lavoie, L.L. Cribbs, S.K. England, C.D. Sigmund, R.M. Weiss, et al. 2003. Abnormal coronary function in mice deficient in alpha1H T-type Ca^{2+} channels. *Science.* 302:1416–1418. http://dx.doi.org/10.1126/science.1089268

Cole, W.C., and D.G. Welsh. 2011. Role of myosin light chain kinase and myosin light chain phosphatase in the resistance arterial myogenic response to intravascular pressure. *Arch. Biochem. Biophys.* 510:160–173. http://dx.doi.org/10.1016/j.abb.2011.02.024

Cui, W., D.D. Taub, and K. Gardner. 2007. qPrimerDepot: a primer database for quantitative real time PCR. *Nucleic Acids Res.* 35 (Database):D805–D809. http://dx.doi.org/10.1093/nar/gkl767

Faraci, F.M., and D.D. Heistad. 1990. Regulation of large cerebral arteries and cerebral microvascular pressure. *Circ. Res.* 66:8–17. http://dx.doi.org/10.1161/01.RES.66.1.8

Filosa, J.A., A.D. Bonev, S.V. Straub, A.L. Meredith, M.K. Wilkerson, R.W. Aldrich, and M.T. Nelson. 2006. Local potassium signaling couples neuronal activity to vasodilation in the brain. *Nat. Neurosci.* 9:1397–1403. http://dx.doi.org/10.1038/nn1779

Frazier, C.J., J.R. Serrano, E.G. George, X. Yu, A. Viswanathan, E. Perez-Reyes, and S.W. Jones. 2001. Gating kinetics of the α1I T-type calcium channel. *J. Gen. Physiol.* 118:457–470. http://dx.doi.org/10.1085/jgp.118.5.457

Fukuda, T., T. Kuroda, M. Kono, T. Miyamoto, M. Tanaka, and T. Matsui. 2014. Attenuation of L-type Ca^{2+} channel expression and vasomotor response in the aorta with age in both Wistar-Kyoto and spontaneously hypertensive rats. *PLoS ONE.* 9:e88975. http://dx.doi.org/10.1371/journal.pone.0088975

Furchgott, R.F., and J.V. Zawadzki. 1980. The obligatory role of endothelial cells in the relaxation of arterial smooth muscle by acetylcholine. *Nature.* 288:373–376. http://dx.doi.org/10.1038/288373a0

Gallagher, P.J., B.P. Herring, and J.T. Stull. 1997. Myosin light chain kinases. *J. Muscle Res. Cell Motil.* 18:1–16. http://dx.doi.org/10.1023/A:1018616814417

Georgeon-Chartier, C., C. Menguy, A. Prévot, and J.L. Morel. 2013. Effect of aging on calcium signaling in C57Bl6J mouse cerebral arteries. *Pflugers Arch.* 465:829–838. http://dx.doi.org/10.1007/s00424-012-1195-7

Giordanetto, F., L. Knerr, and A. Wållberg. 2011. T-type calcium channels inhibitors: a patent review. *Expert Opin Ther Pat.* 21:85–101. http://dx.doi.org/10.1517/13543776.2011.536532

Godfraind, T. 2014. Calcium channel blockers in cardiovascular pharmacotherapy. *J. Cardiovasc. Pharmacol. Ther.* 19:501–515. http://dx.doi.org/10.1177/1074248414530508

Goldman, D., and A.S. Popel. 2000. A computational study of the effect of capillary network anastomoses and tortuosity on oxygen transport. *J. Theor. Biol.* 206:181–194. http://dx.doi.org/10.1006/jtbi.2000.2113

Harraz, O.F., and D.G. Welsh. 2013. Protein kinase A regulation of T-type Ca^{2+} channels in rat cerebral arterial smooth muscle. *J. Cell Sci.* 126:2944–2954. http://dx.doi.org/10.1242/jcs.128363

Harraz, O.F., R.R. Abd El-Rahman, K. Bigdely-Shamloo, S.M. Wilson, S.E. Brett, M. Romero, A.L. Gonzales, S. Earley, E.J. Vigmond, A. Nygren, et al. 2014. $Ca_{(V)}3.2$ channels and the induction of negative feedback in cerebral arteries. *Circ. Res.* 115:650–661. http://dx.doi.org/10.1161/CIRCRESAHA.114.304056

Jensen, L.J., M. Salomonsson, B.L. Jensen, and N.H. Holstein-Rathlou. 2004. Depolarization-induced calcium influx in rat mesenteric small arterioles is mediated exclusively via mibefradil-sensitive calcium channels. *Br. J. Pharmacol.* 142:709–718. http://dx.doi.org/10.1038/sj.bjp.0705841

Knot, H.J., and M.T. Nelson. 1998. Regulation of arterial diameter and wall $[Ca^{2+}]$ in cerebral arteries of rat by membrane potential and intravascular pressure. *J. Physiol.* 508:199–209. http://dx.doi.org/10.1111/j.1469-7793.1998.199br.x

Kumar, S., and R.J. Hall. 2003. Drug treatment of stable angina pectoris in the elderly: defining the place of calcium channel antagonists. *Drugs Aging.* 20:805–815. http://dx.doi.org/10.2165/00002512-200320110-00002

Kuo, I.Y., A. Ellis, V.A. Seymour, S.L. Sandow, and C.E. Hill. 2010. Dihydropyridine-insensitive calcium currents contribute to function of small cerebral arteries. *J. Cereb. Blood Flow Metab.* 30:1226–1239. http://dx.doi.org/10.1038/jcbfm.2010.11

Lee, J.H., J.C. Gomora, L.L. Cribbs, and E. Perez-Reyes. 1999. Nickel block of three cloned T-type calcium channels: low concentrations selectively block alpha1H. *Biophys. J.* 77:3034–3042. http://dx.doi.org/10.1016/S0006-3495(99)77134-1

Li, Z., X. Wang, G. Gao, D. Qu, B. Yu, C. Huang, K.S. Elmslie, and B.Z. Peterson. 2010. A single amino acid change in $Ca_{(v)}1.2$ channels eliminates the permeation and gating differences between $Ca^{(2+)}$ and $Ba^{(2+)}$. *J. Membr. Biol.* 233:23–33. http://dx.doi.org/10.1007/s00232-009-9221-1

Liao, P., D. Yu, G. Li, T.F. Yong, J.L. Soon, Y.L. Chua, and T.W. Soong. 2007. A smooth muscle Cav1.2 calcium channel splice variant underlies hyperpolarized window current and enhanced state-dependent inhibition by nifedipine. *J. Biol. Chem.* 282:35133–35142. http://dx.doi.org/10.1074/jbc.M705478200

Monteil, A., J. Chemin, V. Leuranguer, C. Altier, G. Mennessier, E. Bourinet, P. Lory, and J. Nargeot. 2000. Specific properties of T-type calcium channels generated by the human alpha 1I subunit. *J. Biol. Chem.* 275:16530–16535. http://dx.doi.org/10.1074/jbc.C000090200

Moosmang, S., V. Schulla, A. Welling, R. Feil, S. Feil, J.W. Wegener, F. Hofmann, and N. Klugbauer. 2003. Dominant role of smooth muscle L-type calcium channel Cav1.2 for blood pressure regulation. *EMBO J.* 22:6027–6034. http://dx.doi.org/10.1093/emboj/cdg583

Navedo, M.F., G.C. Amberg, V.S. Votaw, and L.F. Santana. 2005. Constitutively active L-type Ca^{2+} channels. *Proc. Natl. Acad. Sci. USA.* 102:11112–11117. http://dx.doi.org/10.1073/pnas.0500360102

Ogura, C., K. Ono, S. Miyamoto, A. Ikai, S. Mitani, N. Sugimoto, S. Tanaka, and M. Fujita. 2012. L/T-type and L/N-type calcium-channel blockers attenuate cardiac sympathetic nerve activity in patients with hypertension. *Blood Press.* 21:367–371. http://dx.doi.org/10.3109/08037051.2012.694200

Perez-Reyes, E. 2003. Molecular physiology of low-voltage-activated t-type calcium channels. *Physiol. Rev.* 83:117–161. http://dx.doi.org/10.1152/physrev.00018.2002

Pries, A.R., T.W. Secomb, P. Gaehtgens, and J.F. Gross. 1990. Blood flow in microvascular networks. Experiments and simulation. *Circ. Res.* 67:826–834. http://dx.doi.org/10.1161/01.RES.67.4.826

Pries, A.R., T.W. Secomb, T. Gessner, M.B. Sperandio, J.F. Gross, and P. Gaehtgens. 1994. Resistance to blood flow in microvessels in vivo. *Circ. Res.* 75:904–915. http://dx.doi.org/10.1161/01.RES.75.5.904

Segal, S.S. 2000. Integration of blood flow control to skeletal muscle: key role of feed arteries. *Acta Physiol. Scand.* 168:511–518. http://dx.doi.org/10.1046/j.1365-201x.2000.00703.x

Sugano, N., K. Hayashi, T. Hosoya, and T. Yokoo. 2013. Mechanistic view of renal protective action of calcium channel blockade. *Curr. Hypertens. Rep.* 9:187–192. http://dx.doi.org/10.2174/15734021 0903140415124048

Thuesen, A.D., H. Andersen, M. Cardel, A. Toft, S. Walter, N. Marcussen, B.L. Jensen, P. Bie, and P.B. Hansen. 2014. Differential effect of T-type voltage-gated Ca^{2+} channel disruption on renal plasma flow and glomerular filtration rate in vivo. *Am. J. Physiol. Renal Physiol.* 307:F445–F452. http://dx.doi.org/10.1152/ajprenal.00016.2014

Ullrich, N.D., A. Koschak, and K.T. MacLeod. 2007. Oestrogen directly inhibits the cardiovascular L-type Ca^{2+} channel Cav1.2. *Biochem. Biophys. Res. Commun.* 361:522–527. http://dx.doi.org/10.1016/j.bbrc.2007.07.054

Welsh, D.G., M.T. Nelson, D.M. Eckman, and J.E. Brayden. 2000. Swelling-activated cation channels mediate depolarization of rat cerebrovascular smooth muscle by hyposmolarity and intravascular pressure. *J. Physiol.* 527:139–148. http://dx.doi.org/10.1111/j.1469-7793.2000.t01-1-00139.x

Welsh, D.G., A.D. Morielli, M.T. Nelson, and J.E. Brayden. 2002. Transient receptor potential channels regulate myogenic tone of resistance arteries. *Circ. Res.* 90:248–250. http://dx.doi.org/10.1161/hh0302.105662